



U.S. Department of Transportation
Federal Highway Administration

TechBrief

Evaluation of Large-Format Metallic Additive Manufacturing (AM) for Steel Bridge Applications

FHWA Publication No.: FHWA-HIF-24-008

This document is a technical summary of the Georgia Institute of Technology report, *Evaluation of Large-Format Metallic Additive Manufacturing (AM) for Steel Bridge Applications: Final Report of Tensile, Impact, and Fatigue Testing Results* (GT-SEMM-23-01), available at <https://rosap.ntl.bts.gov/view/dot/72366>[1]. This report is a deliverable from a research study sponsored by the Federal Highway Administration (FHWA).

Introduction

Metallic additive manufacturing (AM) can offer an array of positive characteristics: automation, capability to fabricate geometric complexity, component optimization, consolidated assembly, digital inventory, and reduced material waste. Other large-scale metallic industries have realized and applied these advantages, including aerospace, power generation, maritime, and defense [2–5]. Wire arc additive manufacturing (WAAM) is a directed energy deposition (DED) AM process capable of printing using metallic feedstocks, such as traditional welding wire consumables. Advances in WAAM, namely its integration with robotic arms and positioners, allow large-scale components, measured on the scale of feet, to be fabricated [6]. For these reasons, WAAM can be an attractive option for producing large-scale structural components. However, a current lack of fundamental knowledge of the material and fatigue behaviors of WAAM may hinder its widespread adoption in the construction and transportation structure industries.

Notice — This document is disseminated under the sponsorship of the U.S. Department of Transportation in the interest of information exchange. The U.S. Government assumes no liability for the use of the information contained in this document. The U.S. Government does not endorse products or manufacturers. Trademarks or manufacturers' names appear in this document only because they are considered essential to the objective of the document. They are included for informational purposes only and are not intended to reflect a preference, approval, or endorsement of any one product or entity.

Non-Binding Contents — Except for the statutes and regulations cited, the contents of this document do not have the force and effect of law and are not meant to bind the States or the public in any way. This document is intended only to provide information regarding existing requirements under the law or agency policies.

Quality Assurance Statement — The Federal Highway Administration (FHWA) provides high-quality information to serve Government, industry, and the public in a manner that promotes public understanding. Standards and policies are used to ensure and maximize the quality, objectivity, utility, and integrity of its information. FHWA periodically reviews quality issues and adjusts its programs and processes to ensure continuous quality improvement.

FHWA Contact — Justin Ocel, HIT-RC, (202) 281-8213, justin.ocel@dot.gov.

Researchers — This work was conducted by Georgia Institute of Technology under the direction of Dr. Ryan J. Sherman, Hannah D. Kessler, Dr. Karl H. Frank, and Ronnie Medlock. The work was performed under contract 693JJ321C000032.

Key Words — additive manufacturing, wire arc additive manufacturing, tension, impact, fatigue, steel bridge.

Scope

The study had the following objectives:

- Create material property datasets for WAAM ER70S-6 and ER80S-Ni1 filler metal components through tension and Charpy V-notch (CVN) impact tests [7].
- Compare the tension and CVN results to those from the literature, American Welding Society (AWS) A5.18¹ and A5.28² specifications, and American Association of State Highway and Transportation Officials (AASHTO) *Load and Resistance Factor Design (LRFD) Bridge Design Specifications (9th Edition)*⁴ [8–10].
- Determine the influence of the as-fabricated surface finish on the fatigue behavior of WAAM ER70S-6 filler metal components through uniaxial fatigue tests (similar in geometry to those prescribed in ASTM E466-21³ [11]).
- Compare and quantify material property anisotropy with respect to the build and deposition directions of the WAAM components.
- Compare the fatigue performance of the as-fabricated and machined surface finish specimens to the literature and the fatigue detail categories of the AASHTO *LRFD Bridge Design Specifications (9th Edition)*⁴.
- Identify potential WAAM applications in the transportation sector based on the advantages of WAAM and its material and fatigue properties.

Method

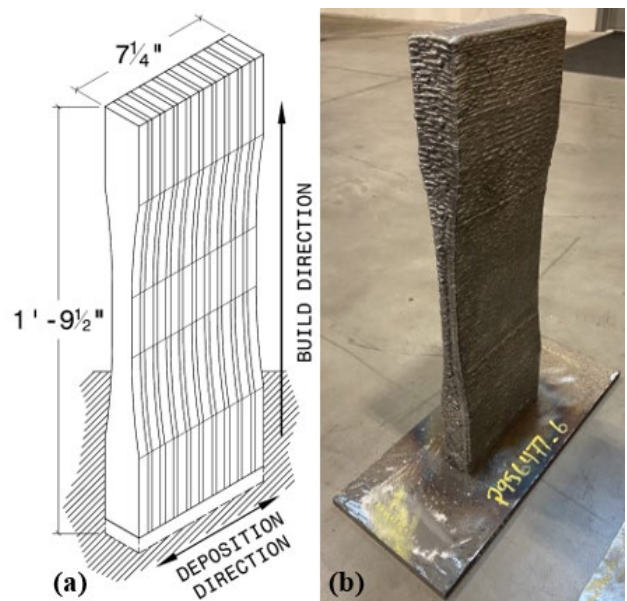
WAAM Components

Traditional filler metal wires, such as those typical for gas metal arc welding processes, are used as the feedstock for WAAM. A shielded arc melts the wire and a single layer of material is deposited. This is repeated until the entire part is formed, leading to a layered component with a ridged surface finish [1,12]. The layers lead to two distinct directions in

the material: the build direction (BD) and the deposition direction (DD). The fabricator of the WAAM components for this study short-circuit transferred the outer beads of each layer and spray transferred the inner beads of each layer.

This study used two different filler metal wires as feedstocks, ER70S-6 and ER80S-Ni1. ER70S-6 was selected because its CVN and tensile properties are aligned with traditional bridge steels, and the literature has shown it to have promising performance as a WAAM feedstock. ER80S-Ni1 was chosen as a feedstock because it is a compatible filler metal for use with uncoated weathering steel (ASTM A709 Grade 50W), and its performance as a WAAM feedstock has yet to be characterized [13].

Two different components were produced for this study: material characterization components were rectangular blocks (also referred to as “walls”) and fatigue components had a rough shape of the fatigue specimens as shown in Figure 1.



Source: FHWA.

Note: units in inches.

Figure 1. Schematic and Photo. Schematic of fatigue component including dimensions (a) and photo of finished near-net component (b).

¹ Use of AWS A5.18, Specification for Carbon Steel Electrodes and Rods for Gas Shielded Arc Welding, is not a Federal requirement.

² Use of AWS A5.28, Low-Alloy Steel Electrodes & Rods for Gas Shielded Arc Welding, is not a Federal requirement.

³ Use of ASTM E466-21, Standard Practice for Conducting Force Controlled Constant Amplitude Axial Fatigue Test of Metallic Materials, is not a Federal requirement.

⁴ FHWA approved the use of the AASHTO LRFD Bridge Design Specifications 9th Edition, although the use is not required (see Memorandum dated April 11, 2022 at <https://www.fhwa.dot.gov/bridge/structures/04112022.pdf>).

The wire type, wire diameter, average heat input for the inner and outer beads, average interlayer temperature, total build time, and shielding gas composition for each wall and fatigue component can be found in the report [1].

Tension and CVN Specimens & Procedure

Four material characterization walls with approximate dimensions of 1 foot 5 ¹¹/₁₆ inches wide by 1 foot 8 inches tall by 1 ¹/₈ inches thick were fabricated using WAAM. Two walls were fabricated using ER70S-6 welding wire feedstock. Of these two walls, one was fabricated with a low interpass temperature (250 °F) and one was fabricated with a high interpass temperature (590 °F). These walls were labeled "F70Lo" and "F70Hi," respectively. Two walls were fabricated using ER80S-Ni1 welding wire feedstock. Of these two walls, one was fabricated with a low interpass temperature (250°F) and one was fabricated with a high interpass temperature (710 °F). These walls were labeled "F80Lo" and "F80Hi," respectively.

Tension Testing

To evaluate tensile properties, sheet-type specimens were manufactured from the four material characterization walls per ASTM A370-22⁵ [7]. Tension coupons were removed from three orientations: longitudinal axis parallel to the BD, longitudinal axis parallel to the DD, and longitudinal axis oriented at a 45° angle to the BD and DD. The approximate locations from which the tension coupons were removed from each material characterization wall are shown in Figure 2. Nine specimens (three in each direction) were tested from walls F70Lo, F70Hi, and F80Hi. Eight specimens (three in the BD, three in 45 directions, and two in the DD) were tested from wall F80Lo. Tension coupon types were labeled in the following format: "WALL ID-ORIENTATION." For example, coupons "F70Lo-BD" are taken from wall F70Lo with their longitudinal axes parallel to the build direction.

The testing machine was set to a crosshead speed equal to 0.003 inches/min, which was acceptable per ASTM A370-22⁵ Section 8.4 [7]. Digital image correlation (DIC) was used during testing to monitor

the full strain field on one side of each specimen and strain was reported using a 2.000-inch virtual extensometer.

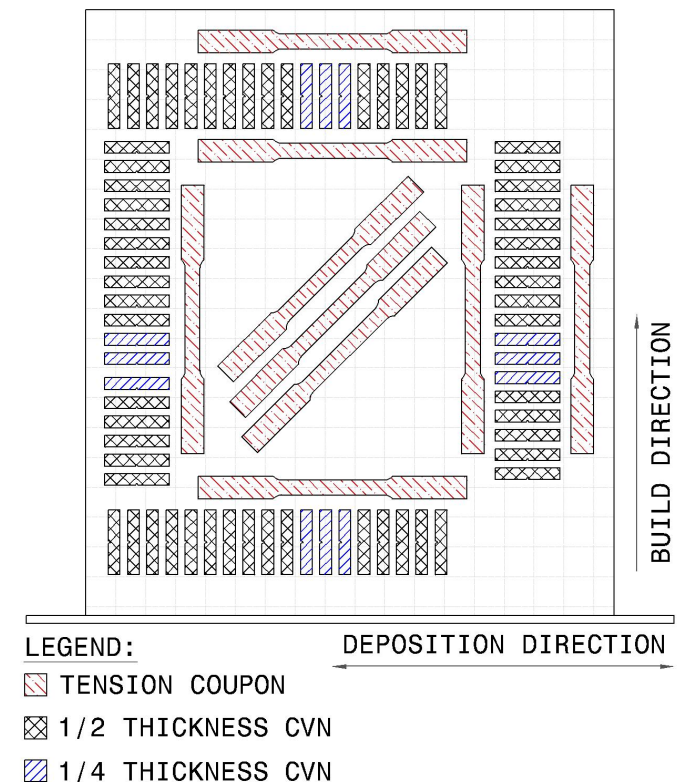


Figure 2. Schematic. Approximate locations of tension, $\frac{1}{2} T$ CVN, and $\frac{1}{4} T$ specimens in each material characterization wall.

CVN Testing

CVN specimens sized according to ASTM A370-22⁵ were extracted from the four walls and tested [7]. The notched face and face opposite of the notch were machined using wire electrical discharge machining, while the remaining two faces were surface ground. CVN specimens were extracted at two points through the thickness of the walls: the middle of the thickness ($\frac{1}{2} T$, nominally ⁹/₁₆ inches from the outer edge of the wall) and the quarter point of the thickness ($\frac{1}{4} T$, nominally ⁹/₃₂ inches from the outer edge of the wall).

CVN specimens were extracted with the notch parallel to the BD and parallel to the DD. The approximate locations from which the CVN specimens were removed from each material

⁵ Use of ASTM A370-22, Standard Test Methods and Definitions for Mechanical Testing of Steel Products, is not a Federal requirement.

characterization wall are shown in Figure 2. A total of 272 CVN specimens were tested. CVN specimen types were labeled in the following format: "WALL ID-NOTCH ORIENTATION." For example, specimens "F70Lo-BD" are taken from wall F70Lo with their notches parallel to the BD (i.e., longitudinal axis perpendicular to the DD).

Sets of two to four $\frac{1}{2} T$ specimens of each orientation (i.e., BD and DD) from each wall were tested at seven temperature levels (i.e., -110, -90, -60, -30, 10, 40, and 70 °F) to develop the full temperature-transition curve. Sets of three to six $\frac{1}{4} T$ specimens were tested at -30 °F. All specimens were tested in accordance to ASTM A370-22⁵ [7]. The measured absorbed energy was recorded as each specimen was broken.

Fatigue Specimens & Procedure

Four fatigue components were fabricated using ER70S-6 welding wire feedstock: two with a low interpass temperature (250 °F) and two with a high interpass temperature (750 °F). One of the builds fabricated at each interpass temperature was fabricated close to the final specimen cross-section to test the as-built surface finish. The other build fabricated at each interpass temperature was fabricated with 0.2 inches added to each dimension of the cross section such that the as-built surface finish could be fully machined away. Specimens were labeled in the following format: "INTERPASS TEMP.-SURFACE FINISH." For example, specimen Hi-AB is taken from the high interpass component with an as-built surface finish.

The as-built surface finish specimens were hand-finished, leading to an undercut of the gauge length. Because the width of the gauge length of the as-built specimens was undercut, DIC was used to evaluate the strain field at the transition and the gauge length in addition to a strain gauge. At least 90 cycles were applied to the as-built specimens, and no stress concentrations at the undercut area were noted. Similarly, at least 90 cycles of load were applied to the machined specimens to verify that the correct stress range was achieved in the gauge length. Figure 3 shows the finished cross-sections of the machined and as-built fatigue specimens.

Specimens were cyclically loaded in uniaxial tension in a universal test machine. Stress range cycles were applied in a sinusoidal waveform to the specimens at a rate of 15 Hz for all stress ranges except the 38 ksi stress range, which was applied at 12 Hz.



Source: FHWA.

Figure 3. Photo. Finished cross-sections of the machined and as-built fatigue specimens.

Results & Discussion

Tension Testing

Figure 4 compares the engineering stress-strain diagrams for all specimens from the four walls. Table 1 shows each wall's average yield strength, tensile strength, and elongation at fracture in the BD, DD, and 45 directions. The ratios between each specimen direction (i.e., BD, DD, and 45) with respect to each of the other directions for average tensile strength, average yield strength, and average percent elongation at fracture are in Table 2.

Generally, the difference between the three directions for tensile and yield strength was low, with ratios ranging from 0.95 to 1.05. The difference between the three directions for percent elongation at fracture

was more variable, with ratios ranging from 0.76 to 0.97. The smallest ratios of percent elongation at fracture for all walls were 45° over DD ratios. The largest ratios of percent elongation at fracture for

walls F70Lo, F80Lo, and F80Hi were 45° over BD ratios. The largest ratio of percent elongation at fracture for wall F70Hi was the BD over DD ratio.

Table 1. Average yield strength, tensile strength, and elongation at fracture in the BD, DD, and 45° directions for each wall.

Wall	BD Yield Strength (ksi)	DD Yield Strength (ksi)	45° Yield Strength (ksi)	BD Tensile Strength (ksi)	DD Tensile Strength (ksi)	45° Tensile Strength (ksi)	BD Elongation at Fracture (%)	DD Elongation at Fracture (%)	45° Elongation at Fracture (%)
F70Lo	56.4	58.8	59.0	73.0	73.9	74.3	35.3	40.9	32.3 [^]
F70Hi	45.8	48.1	46.4	65.1	66.1	65.2	43.5	45.1	38.2
F80Lo	59.1	61.7	61.2	77.1	77.9	77.8	33.5	38.8	29.4
F80Hi	51.7	52.7	51.4	71.1	71.1	71.0	39.8	42.5*	38.6

[^]Average determined without the elongation at fracture of one specimen which was tested on an unaligned test machine.

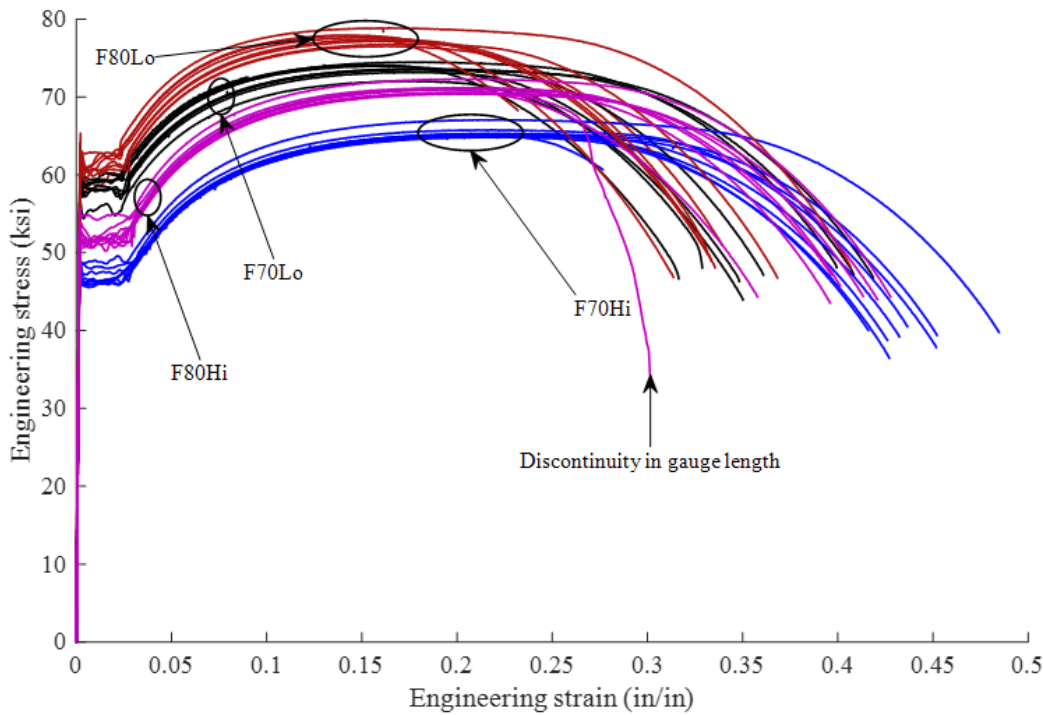
*Average determined without the elongation at fracture of one specimen which had an internal discontinuity in its gauge length.

Table 2. Tensile result comparison between directions tested.

Wall	BD/DD Yield Ratio	45°/BD Yield Ratio	45°/DD Yield Ratio	BD/DD Tensile Ratio	45°/BD Tensile Ratio	45°/DD Tensile Ratio	BD/DD Elongation at Fracture Ratio	45°/BD Elongation at Fracture Ratio	45°/DD Elongation at Fracture Ratio
F70Lo	0.96	1.05	1.00	0.99	1.02	1.00	0.86	0.91 [^]	0.79 [^]
F70Hi	0.95	1.01	0.96	0.99	1.00	0.99	0.96	0.88	0.85
F80Lo	0.96	1.04	0.99	0.99	1.01	1.00	0.86	0.88	0.76
F80Hi	0.98	1.00	0.98	1.00	1.00	1.00	0.94*	0.97	0.91*

[^]Average determined without the elongation at fracture of one specimen which was tested on an unaligned test machine.

*Average determined without the elongation at fracture of one specimen which had an internal discontinuity in its gauge length.



Source: FHWA.

Figure 4. Graph. Engineering stress-strain diagrams for all specimens.

Interpass temperature had the most significant influence on the yield and tensile strengths of the evaluated WAAM material. The ER70S-6 and ER80S-Ni1 WAAM materials produced with a low interpass temperature had higher average yield and tensile strengths. Conversely, on average, the low interpass temperature materials had lower percent elongation at fracture (i.e., lower ductility).

Comparisons were drawn to material properties listed in AWS A5.18¹ and A5.28². However, it should be noted that the gas compositions tested in the current study did not match that used in the classification; as such, deviations in strength and elongation at fracture can be expected. The material properties listed in AWS 5.18¹ are 58 ksi yield strength, 70 ksi tensile strength, and 22 percent elongation at fracture. The material properties listed in by AWS 5.28² are 68 ksi yield strength, 80 ksi tensile strength, and 24 percent elongation at fracture.

The average of DD and 45 specimens from F70Lo met the minimum yield strength of AWS A5.18¹; however, the average BD specimen did not meet the minimum yield strength. All of the average specimens from F70Lo met the listed tensile strength. None of the average specimens from F70Hi met the listed yield or tensile strength. None of the average specimens from F80Lo met the listed yield or tensile strength. None of the average specimens from F80Hi met the listed yield or tensile strength. All average specimens from all directions and all walls met the listed elongation (not including two specimens which were redacted from the dataset).

CVN Testing

Figure 5 plots the temperature versus impact energy for the $\frac{1}{2} T$ BD specimens for all four walls. Figure 6 plots the temperature versus impact energy for the $\frac{1}{2} T$ DD specimens for all four walls. Five parameter sigmoid fits for each specimen type are also included.

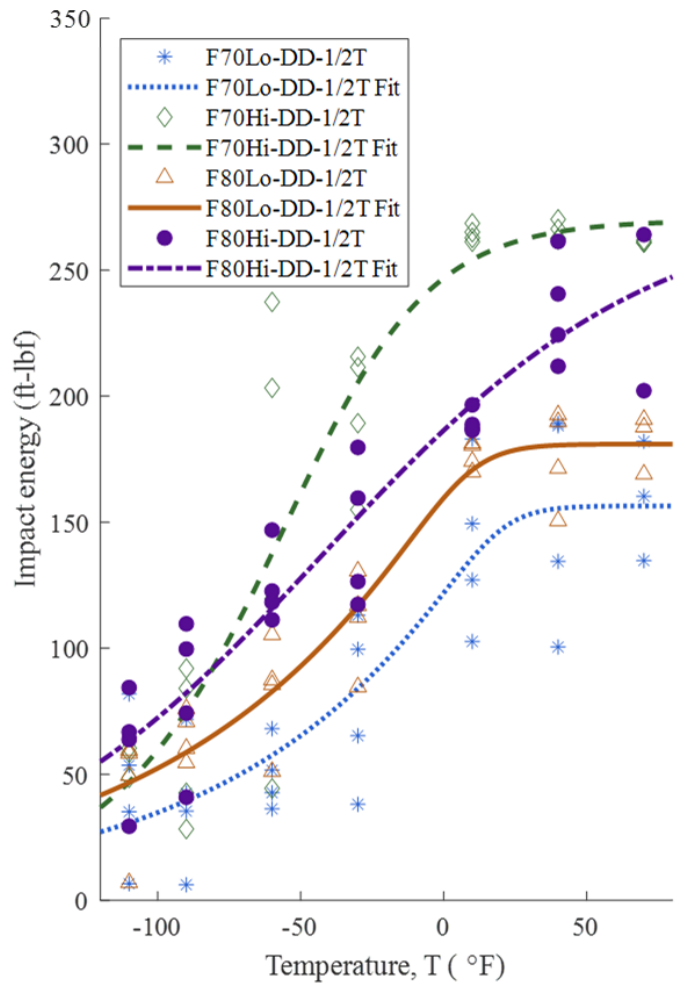
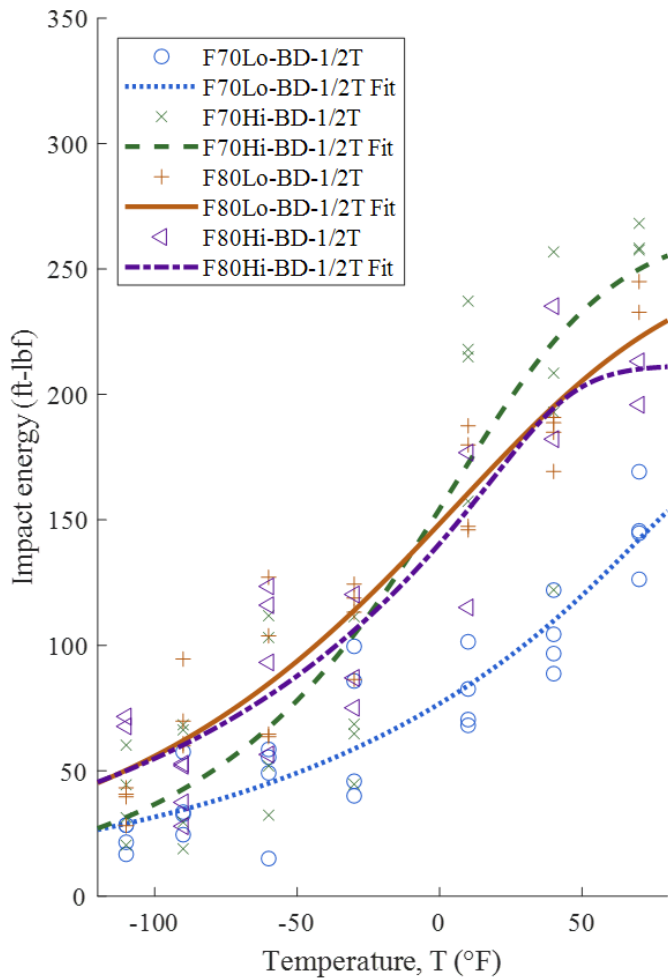
The sigmoid fits of the DD specimens from walls F70Lo, F70Hi, and F80Lo show similar trends to each other. They have the distinct upper and lower shelves expected from body-centered cubic metals,

and all appear to have a ductile-to-brittle transition temperature between -90 °F and 10 °F. The sigmoid fits of the BD specimens from walls F70Lo, F70Hi, and F80Lo also show similar trends to each other. They do not have distinct upper shelves over the range of temperatures tested and do not have an obvious ductile-to-brittle transition temperature. Wall F80Hi demonstrates the opposite behavior, a distinct upper shelf is not observed in the DD specimens over the range of temperatures tested but is observed in the BD specimens. The DD specimens do not demonstrate any clear trend regarding the F70 versus F80 specimens, resulting in higher absorbed energies. Generally, the F80 DD specimens have absorbed energies between the absorbed energies of the F70Lo and F70Hi DD specimens.

The higher interpass temperature generally yielded higher impact energies than the corresponding lower interpass temperature. For the BD specimens, both high interpass temperature sets of specimens showed distinct upper shelves, whereas the low interpass temperature sets of specimens did not. For the DD specimens, the same correlation between the interpass temperature and the presence of an upper shelf does not exist.

Table 3 summarizes the ratios between the average absorbed energies in the BD and DD. Most of the ratios for the F70Lo, F70Hi, and F80Hi specimens are less than 1.0, meaning that the impact energy in the BD was less than that in the DD. The majority of the ratios for these walls were less than 0.9, indicating that the behavior may be anisotropic. Most of the ratios for the F80Lo wall were greater than 1.0, meaning that the impact energy in the BD was greater than that in the DD. The majority of the ratios for this wall were between 0.9 and 1.1, indicating more isotropic behavior.

Results for $\frac{1}{4} T$ specimens can be found in the full report [1]. All CVN specimens tested between 10 °F and 70 °F exceeded the minimum value per AASHTO *LRFD Bridge Design Specifications*⁴ for non-fracture critical (15 ft-lbf) and fracture critical members (25 ft-lbf).



Source: FHWA.

Source: FHWA.

Figure 5. Graph. Temperature versus impact energy for BD $1/2 T$ specimens from all material characterization walls.

Figure 6. Graph. Temperature versus impact energy for DD $1/2 T$ specimens from all material characterization walls.

Table 3. Ratios between the average absorbed energies of the BD and DD specimens for each wall.

Temperature (°F)	F70Lo Average Impact Energy Ratio, BD/DD	F70Hi Average Impact Energy Ratio, BD/DD	F80Lo Average Impact Energy Ratio, BD/DD	F80Hi Average Impact Energy Ratio, BD/DD
-110	0.53	0.70	0.87	1.14
-90	0.95	0.74	1.09	0.52
-60	0.90	0.49	1.09	0.78
-30	0.86	0.37	1.00	0.65
10	0.57	0.78	0.94	0.77
40	0.67	0.74	1.04	0.89
70	0.92	1.00	1.31	0.88

Fatigue Testing

As-built specimens were tested at three stress ranges: 12, 16, and 20 ksi. Machined specimens were tested at two different stress ranges: 30 and 38 ksi. Figure 7 shows the S-N plot for the as-built specimen data and the corresponding 95 percent confidence interval regressions compared to the design life AASHTO *LRFD Bridge Design Specifications*⁴ fatigue detail categories [10]. Figure 8 shows the S-N plot for the machined specimen data and the corresponding mean regression compared to the upper bound of AASHTO fatigue detail Category A.

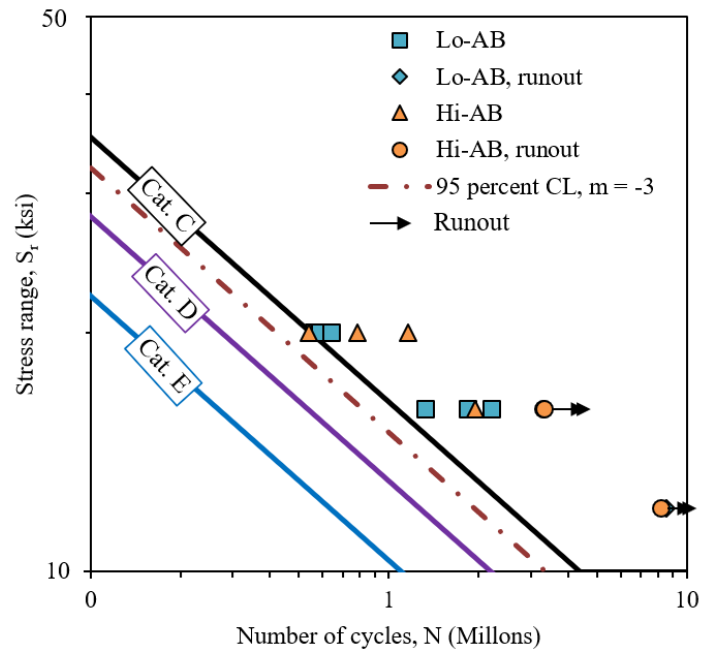
The as-built specimens demonstrated lower fatigue performance than the machined specimens. All machined specimens exceeded AASHTO fatigue detail Category A, with all tested specimens considered runouts. Conversely, except for one specimen, the tested values of the as-built specimens exceeded the design life curve for detail Category C.

The Lo-AB specimens demonstrated slightly lower fatigue performance than the Hi-AB specimens. However, the small number of specimens evaluated was insufficient to quantify the marginal difference. In general, there does not appear to be a difference in surface finish or performance that would warrant a change in the fatigue category based on the interpass temperature; therefore, regression analyses were performed that treated both Hi-AB and Lo-AB specimens as part of one dataset (Figure 7).

A best-fit log-log regression for the mean of the AB specimens tested was determined by a linear least squares approach excluding all runouts. The best-fit regression was adjusted to a 95 percent confidence limit (CL) by shifting the value of the detail constant, A , down by 1.96 standard deviations and fixing the slope to 3.0 to be consistent with the AASHTO design curves [12,14]. The 95 percent CL regression with a slope of 3.0 falls between the design life regressions for Category C and Category D; thus, the AM AB finish would be a Category D detail.

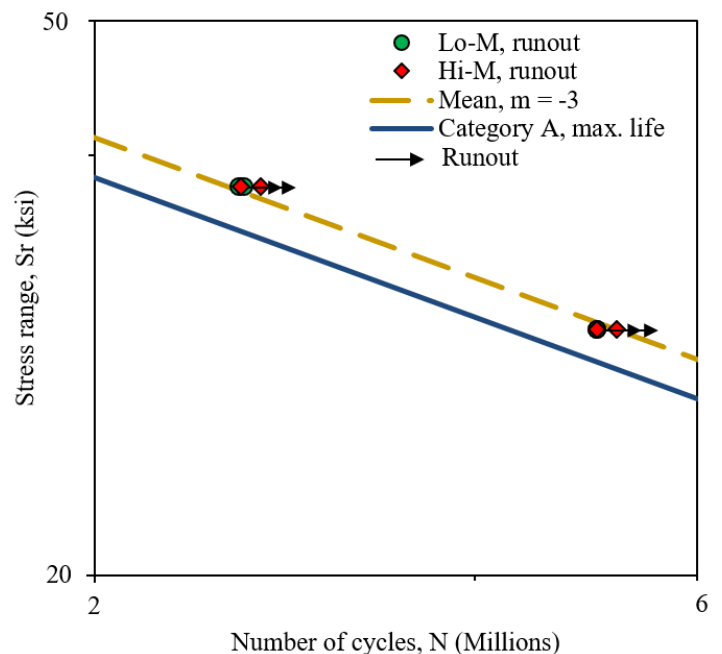
A similar regression for the M specimens was unnecessary as the specimens were considered runouts shortly after they exceeded the adjusted maximum life for Category A. As a result, the slope, m , was forced to equal 3.0 and the mean of the tested specimens to fall above the design life curve for

detail Category A and thus for design a machined finish would be considered Category A.



Source: FHWA.

Figure 7. Graph. S-N plot of as-built specimen data and corresponding 95 percent confidence limit regressions compared to design life AASHTO detail categories.



Source: FHWA.

Figure 8. Graph. S-N plot of machined specimen data and the corresponding mean regression compared to the upper bound of AASHTO detail Category A.

Potential Bridge Applications of AM

Several potential WAAM applications were identified within the transportation sector based on the advantages of WAAM and the results of the tension, impact, and fatigue testing conducted in the current study. This list of components or applications (abbreviated version in Table 4) was created by considering a variety of factors, including current state of WAAM technology, perceived risk by owners, loading scenario complexity, benefits to optimization, fabrication difficulty by traditional means, uniqueness, and component repetition. A score (i.e., 1, 2, or 3) for traditional fabrication difficulty and for benefit to optimize is provided for each component. Scores of 1, 2, and 3 represent low, medium, and high traditional fabrication difficulty or benefit to optimize, respectively. The components or applications listed in Table 4 are ordered by the sum of the fabrication and optimization scores. For the full list of components and a summary of the opportunities and challenges for each component or application, reference the full report [1].

Conclusions

Tension Testing

- No significant anisotropy was observed in the yield and tensile strengths of the WAAM material resulting from both filler metal classifications and both interpass temperatures.
- Percent elongation at fracture is significantly influenced by specimen and load orientation with respect to the BD and DD. The specimens with gauge lengths and loading parallel to the DD generally had higher percent elongations at fracture than those with gauge lengths and loading parallel to the BD and those at a 45° angle between the BD and DD.
- The ER70S-6 and ER80S-Ni1 WAAM materials produced with a low interpass temperature had higher yield and tensile strengths than their counterparts with high interpass temperatures. However, as in the above elongation at fracture results, the lower interpass temperature specimens were less ductile than the high interpass temperature specimens on average.

- The minimum yield and tensile strength in AWS A5.18 for ER70S-6 were met by most of the F70Lo specimens but none of the F70Hi specimens. The minimum yield and tensile strength in AWS A5.28 for ER80S-Ni1 were not met by any of the F80Lo or F80Hi specimens.

CVN Testing

- All impact specimens tested exceeded the AASHTO Grade 50 fracture critical and non-fracture critical limits for all service temperature zones.
- The BD over DD impact energy ratios for the F70Lo, F70Hi, and F80Hi walls were generally less than 0.9 for most temperatures, suggesting their impact energy has some slight anisotropy. The BD over DD impact energy ratios for the F80Lo wall were generally between 0.9 and 1.1, suggesting that this wall had more isotropic behavior.
- There was less scatter between the results for all walls at lower temperatures, with the lowest range of 73 ft-lbf observed at -110 °F. The highest range of 222.4 ft-lbf was observed at -60 °F. Generally, the F70Lo-BD specimens had the lowest absorbed energies, and the F70Hi-DD had the highest absorbed energies.
- The F70Lo, F70Hi, and F80Hi BD specimens did not show a distinct upper shelf over the range of temperatures tested. The F70Lo, F70Hi, and F80Hi DD specimens did show distinct upper and lower shelves. This trend is reversed for the F80Lo specimens.

Fatigue Testing

- For purposes of design, as-built WAAM surfaces would be AASHTO Category D.
- For purposes of design, machined WAAM surfaces would be AASHTO Category A.
- WAAM components have the flexibility to be locally thickened during design to reduce stress ranges to Category D or less and thus the as-built finish can be tolerable. However, if local thickening is not possible, machining the WAAM surface can provide Category A fatigue resistance. Machining may also be performed for aesthetic purposes.

Table 4. List of potential components or applications for WAAM in the transportation sector.

Component or Application	Traditional Fabrication Difficulty Score*	Benefit to Optimize Score*	Sum
Cable saddle (suspension bridge)	3	3	6
Rapid prototyping	3	3	6
Stay cable anchorage	3	3	6
Stiffened steel (waffle) hanger connection	3	3	6
TKY connection (tubular members)	2	3	5
Movable bridge casting replacement	3	2	5

*Scores of 1, 2, and 3 represent low, medium, and high traditional fabrication difficulty or benefit to optimize, respectively.

References

- [1] R.J. Sherman, H.D. Kessler, K.H. Frank, R. Medlock, Evaluation of Large-Format Metallic Additive Manufacturing (AM) for Steel Bridge Applications: Final Report of Tensile, Impact, and Fatigue Testing Results, Georgia Institute of Technology, 2023.
- [2] T. DeRoy, H.L. Wei, J.S. Zuback, T. Mukherjee, J.W. Elmer, J.O. Milewski, A.M. Beese, A. Wilson-Heid, A. De, W. Zhang, Additive manufacturing of metallic components – Process, structure and properties, *Progress in Materials Science*. 92 (2018) 112–224. <https://doi.org/10.1016/j.pmatsci.2017.10.001>.
- [3] M. Douglass, Addressing Production Challenges and Go-to-Market Limitations with Established Additive Manufacturing Service Providers, 2020.
- [4] ADDere, Getting Structural Scale Metal Parts to Market Faster: How ADDere Manufacturing dramatically reduced time and material cost by 3D printing large, high mass components, Midwest Engineered Systems, 2021.
- [5] T. Lehmann, D. Rose, E. Ranjbar, M. Ghasri-Khouzani, M. Tavakoli, H. Henein, T. Wolfe, A. Jawad Qureshi, Large-scale metal additive manufacturing: a holistic review of the state of the art and challenges, *International Materials Reviews*. 67 (2022) 410–459. <https://doi.org/10.1080/09506608.2021.1971427>.
- [6] A. Nycz, A.I. Adediran, M.W. Noakes, L.J. Love, Large scale metal additive techniques review, in: *Proceedings of the 27th Annual International Solid Freeform Fabrication Symposium*, 2016.
- [7] ASTM International, ASTM A370-22: Standard Test Methods and Definitions for Mechanical Testing of Steel Products, 2022.
- [8] American Welding Society, A5.18/A5.18M:2021: Specification for Carbon Steel Electrodes and Rods for Gas Shielded Arc Welding, American National Standards Institute, 2021.
- [9] American Welding Society, A5.28/A5.28M:2022: Specification for Low-Alloy Steel Electrodes and Rods for Gas Shielded Arc Welding, 2020.
- [10] AASHTO, LRF Bridge Design Specifications, American Association of State Highway and Transportation Officials, 2020.
- [11] ASTM International, ASTM E466-21: Standard of Practice for Conducting Force Controlled Constant Amplitude Axial Fatigue Tests of Metallic Materials, 2021.
- [12] P.B. Keating, J.W. Fisher, Review of fatigue tests and design criteria on welded details, final report, Lehigh University, 1986.
- [13] ASTM International, ASTM A709/A709M-21: Standard Specification for Structural Steel for Bridges, 2021.
- [14] Strategic Highway Research Program, Bridges for Service Life Beyond 100 Years: Service Limit State Design, Transportation Research Board, Washington, D.C., 2014. <https://doi.org/10.17226/22441>.